Structure of colloidosomes with tunable particle density: Simulation versus experiment

Riccardo Fantoni,[1,*] Johannes W. O. Salari,[2,†] and Bert Klumperman[2,3,‡]

[1]*National Institute for Theoretical Physics and Institute of Theoretical Physics, University of Stellenbosch, Stellenbosch 7600, South Africa*

[2]*Department of Polymer Chemistry, University of Technology Eindhoven, P.O. Box 513, 5600 MB Eindhoven, The Netherlands*

[3]*Stellenbosch University, Department of Chemistry and Polymer Science, Private Bag X1, 7602 Matieland, South Africa*

(Received 14 February 2012; published 6 June 2012)

Colloidosomes are created in the laboratory from a Pickering emulsion of water droplets in oil. The colloidosomes have approximately the same diameter and by choosing (hairy) particles of different diameters it is possible to control the particle density on the droplets. The experiment is performed at room temperature. The radial distribution function of the assembly of (primary) particles on the water droplet is measured in the laboratory and in a computer experiment of a fluid model of particles with pairwise interactions on the surface of a sphere.

DOI: 10.1103/PhysRevE.85.061404 PACS number(s): 83.80.Hj, 68.65.−k, 64.70.pv, 64.75.Xc

I. INTRODUCTION

Colloidosomes are hollow spherical structures that are formed by the assembly of colloidal particles at the interfaces of two immiscible liquids [1]. As a result the particles are arranged in a shell that is inherently porous.

The assembly of colloidal particles at liquid interfaces is used in various applications [2]. Moreover, it is a promising technique for the synthesis of novel materials [3] and has recently led to the development of colloidosomes [1], nanocomposite particles [4], porous solids [5], and foams [6].

In this work, we study colloidosomes that are composed of uncharged spherical polystyrene particles of μm size moving on the surface of a water droplet in oil. Similar studies have also been done with charged particles [7]. The study of particles on the surface of a sphere dates back to the old Thomson problem [8] for classical electrons. The statistical physics problem of a one-component plasma on a sphere has been solved exactly analytically at a special value of the temperature [9]. Nonpointwise particles on a sphere have the additional complication of the geometrical frustration, which can be described through the so-called grain boundary scars [10–12]. There have been attempts to formulate a statistical geometry of particle packing [13]. These systems opened up a field of research that studies the effect of curvature and topology of various surfaces on the organization of matter in a more general sense [14]. Structuring at the surface of a droplet can be viewed as a two-dimensional analog to fluid like behavior, crystallization, or glass formation in three-dimensional systems [15].

Fluids on Riemannian surfaces have been the subject of various studies with few exact analytical results [9,16,17], some approximate theories [18], and many Monte Carlo (MC) simulations [19]. Colloidosomes with tunable particle density were synthesized experimentally [20]. A sintering procedure is then used to create capsules, which can be easily handled. The capsules are then dried to obtain colloidal cages. The synthetic details are explained in the next section.

In this work we give the simplest statistical physics description of the colloidosome, where we describe the interaction of the colloidal particles with the surrounding media, water and oil, simply as a holonomic constraint on the particles positions to stay at the water-oil (WO) interface and treat them as a fluid of a fixed number of particles moving on a sphere, the droplet of water in oil, with a mutual pairwise interaction, the pair potential, at a temperature T. Additional frictional effects have been neglected [21]. The assembly of particles on the sphere is studied both in the laboratory and with a computer experiment under certain conditions: number density and temperature. The structural arrangement of the particles is characterized through the radial distribution function. The colloidal particles created in our laboratory are polystyrene solid spherical hairy particles with controllable diameter of the order of 3 μm. The particles will then exhibit a hard core interaction. Two types of particle pair potentials were used in the Monte Carlo (MC) simulation of the fluid, namely the hard-sphere one and the polarizable hard-sphere one.

The work is organized as follows: in Sec. II the colloidosome is described; in Sec. III the radial distribution function as a means to probe the structure of the colloidosome is presented in its mathematical definition described in Appendix A, its MC estimator, and its experimental measure; in Sec. IV the MC simulation results are presented; in Sec. V the theoretically exact results of the MC simulation and the experimental results are compared; Section VI is devoted to concluding remarks.

II. EXPERIMENTAL SYSTEM VERSUS STATISTICAL PHYSICS PROBLEM

The details for the synthesis of the colloidosomes can be found in our previous work [20]. Working at room temperature, we first disperse the colloidal particles in a hydrocarbon oil (heptane). Then, water is added while the solution is being stirred vigorously. The function of the shear is two fold. It causes the water to break up into small water droplets and at the same time it allows to overcome the barrier for adsorption of the particles, which are assembled randomly at the WO interface of the droplets. Eventually a stable Pickering emulsion [22] of water droplets covered by polystyrene (pS) particles, the colloidosomes, in oil is formed. The colloidosomes formed have all approximately

*rfantoni@ts.infn.it
†jorissalari@gmail.com
‡bklump@sun.ac.za

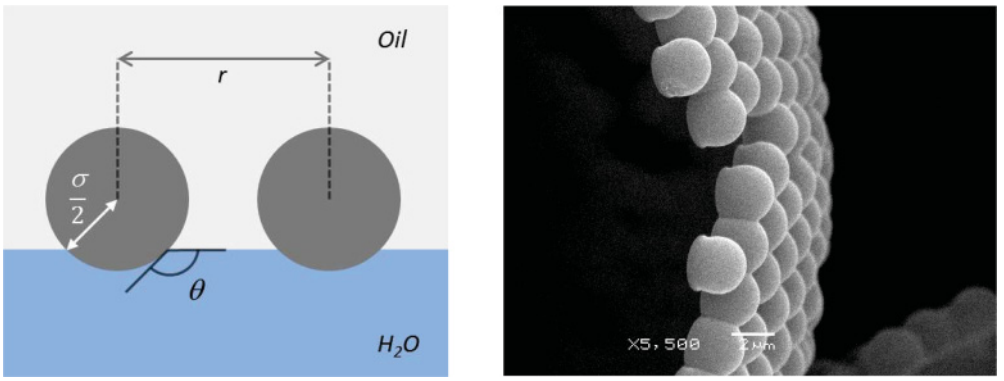

FIG. 1. (Color online) The left panel shows a schematic representation of the equilibrium position of the particles at the WO interface; θ is the three-phase contact angle, r is the particle separation, and σ is the particle diameter. The right panel shows a side view of the particle shell of a colloidosome made with scanning electron microscopy.

the same diameter, and this, as well as the number of colloidal particles on each colloidosome, does not change after the colloidosomes are formed. For further imaging with scanning electron microscopy (SEM) the particles surrounding the droplets need to be (partially) sintered in order to form a continuous and stable shell around the droplet, a capsule. Heating the mixture to 35 °C for 30 minutes proved sufficient to do so. A small amount of the sintered colloidosome dispersion is placed on the SEM sample holder and dried in the fumehood. This removes both the water and heptane remnants and leaves only the capsules, the colloidal cages, which can then be imaged by SEM.

The colloidal polystyrene solid particles are synthesized by the dispersion polymerization of styrene in alcohol and water [20], which is a well-established technique for the formation of highly uniform polymer particles with a narrow size polydispersity. AIBN [azo-bis(isobutyronitrile)] is used as the initiator. The presence of a polymeric stabilizing surface functional group is required for a controlled synthesis of the particles. A nonionic polymeric stabilizer [poly(N-vinylpyrrolidone) (pVP)] is used for this study. Hence, there is no charge on the surface of the particles. During the polymerization, pVP, which efficiently adsorbs on polystyrene, is attached to the particle. In ethanol and water, pVP is soluble. The polymeric chains are extended (with a radius of gyration of $R_g \approx 15$ nm) and are responsible for steric repulsion as two particles get in close contact. This guarantees the steric stabilization of the colloidal suspension. In the oil phase, pVP is insoluble and the polymer chains are collapsed on the surface of the particle, resulting in an attractive potential among the particles. The final dispersion in ethanol and water, therefore, consists of polystyrene particles that are sterically stabilized with a layer of pVP. During the polymerization of styrene, pVP attaches to the particle by both physical adsorption to the particle's surface and chemical grafting. These two mechanisms occur simultaneously, however it is not known to what extent. It is believed that the predominant mechanism for stabilization is the physical adsorption. The particles are washed with pure ethanol by three centrifugation-redispersion cycles in order to remove the residual physically adsorbed pVP. The particles settle due to the centrifugation. The supernatant solution is decanted and clean ethanol is added to the remaining particles. The particles are then redispersed and the whole procedure is repeated three times. The physically adsorbed pVP is removed, which produces a lower colloidal stability of the particles in ethanol. Large aggregates were observed during this procedure, which is an indication for the presence of an attractive component in the pair potential between the colloidal particles in the suspension. The chemically grafted pVP remains attached to the particle's surface. The remaining particles are dried and redispersed in heptane, before the colloidosomes are synthesized. In conclusion, the surface chemical properties of the particles are mainly determined by polystyrene and the fraction of pVP that is chemically grafted to the surface, although a precise estimate of the grafting density is lacking. It is believed that the grafting density is low, due to the poor colloidal stability of the particles in ethanol after removing the physically adsorbed pVP.

In Pickering emulsions, the particle is adsorbed at the WO interface and is partly immersed in the oil and water phase. The extent of immersion in both phases will eventually have an influence on the particle pair potential. The three-phase contact angle θ is used to denote the position at the interface as shown in Fig. 1.[1] It was determined in our earlier work [20] and is approximately $\theta \approx 130^\circ$, which means that the particle is predominantly immersed in the oil. The surface tension of the particle is altered by the presence of the surface stabilizing groups, which affects the wetting properties and the equilibrium position of the particles at the interface [23]. An atomistic [24] level of description of the core of the solid hairy particles suggests the use of Hamaker [25] calculation for the determination of the interaction between the two spherical cores. The calculation predicts an attractive pair potential which, neglecting the detailed behavior close to contact, is proportional to $(\sigma/r)^6$, r being the distance between the centers of the two cores of diameter σ. Unlike this attraction, which is always present, the steric

[1]The right panel of Fig. 1 shows clearly flattening of the particles on the inside of the capsules. We are convinced that this is an artifact of the sintering process. During this process flattening of the particles occurs, which we ascribe to particle deformation to reduce the contact area between particle and water.

repulsion will have a very small range when θ is obtuse since in this case the particle's contact occurs in the oil phase [26]. We thus expect the balance between the attractive interaction and the steric effects to depend on the angle θ. Moreover other kinds of interactions such as depletion, hydrophobic, solvation, or capillary should be taken into account for an accurate description of our system. The simplest description for the pair potential between the particles is the hard-spheres one.

The surface of a sphere of diameter $D = 2R$ is $A = \pi D^2$. The surface area that a particle, with diameter σ, can occupy is approximately $a = \sqrt{3}\sigma^2/2$. The maximum number of particles that can pack the surface of a sphere is approximately

$$N_{\max} \lesssim \frac{A}{a} = \frac{2\pi}{\sqrt{3}} \left(\frac{D}{\sigma}\right)^2, \tag{1}$$

where we assumed that the particles are in a close packing regular hexagonal lattice neglecting curvature effects. The maximum reduced particle density on the sphere will then be $\rho_{\max}\sigma^2 \lesssim 2/\sqrt{3} \approx 1.155$.

Similar experiments [27] make use of water and a liquid of higher density, for the initial solution of the two immiscible liquids. The droplets in the emulsion will now be of the higher density liquid. In the limit of droplets of very high density the particles are expected to be essentially unable to move on the droplet. Our working hypothesis will be, instead, to consider the particles as moving freely on the droplet surface, completely neglecting the presence of the solvent. We then treat the colloidosome of diameter D, number of particles N, and temperature T, through a canonical ensemble classical statistical physics description of the assembly of particles on the water droplet as a fluid of particles constrained to move on the surface of a sphere with a pairwise interaction, the pair potential.

A. Pair potential

Fixing the pair potential completely defines the fluid model, as described in Appendix A and Eq. (8).

The simplest interaction between two colloidal particles is the hard-spheres (HS) pair potential

$$\phi_{\rm HS}(r) = \begin{cases} +\infty & r < \sigma \\ 0 & r > \sigma \end{cases}, \tag{2}$$

where σ is the diameter of the spheres and r is the Euclidean center to center distance [see Eq. (5)].

The interaction between two neutral particles far apart is dominated by dipolar forces. The simplest model potential, suggested by the London forces [28], corresponds to hard spheres of diameter σ with dispersion attractions, the polarizable hard spheres (PHS),

$$\phi_{\rm PHS}(r) = \begin{cases} +\infty & r < \sigma \\ -\epsilon_{\rm PHS}\left(\frac{\sigma}{r}\right)^6 & r > \sigma \end{cases}, \tag{3}$$

where $\epsilon_{\rm PHS} = A^H/36$ is a positive energy proportional to Hamaker constant [25] A^H, which is a property of the material of which the particles are made and of the environment where the particles are immersed. We here neglect the details of Hamaker's macroscopic approximation [28], which when the two spheres are close to contact predicts a $-(A^H/24)/(r/\sigma - 1)$ behavior, as we believe they have not much influence on the calculation.

III. RADIAL DISTRIBUTION FUNCTION

In this work we probed the structure of the colloidosome using the radial distribution function (RDF). We compare the experimental RDFs with the ones obtained from MC simulations of a fluid of particles moving on a sphere and interacting with a model pair-potential of the kinds described in Sec. II A. This procedure will allow us to determine which interaction model best describes the experimental assembly of particles. Choosing σ as the unit length, the statistical physics problem only depends on the number of particles N and the reduced density $\rho\sigma^2 = N/[\pi(D/\sigma)^2]$ for the athermal HS model and also on the reduced temperature $k_BT/\epsilon_{\rm PHS}$ for the PHS one.

A. Monte Carlo simulation

On a sphere, the Monte Carlo simulation [29] solves exactly the statistical physics problem as, since one does not have the additional thermodynamic limit problem, it reduces to an integration, as described in Appendix B.

The particle's positions are $\mathbf{R} = (\mathbf{r}_1, \mathbf{r}_2, \ldots, \mathbf{r}_N)$ with

$$\mathbf{r}_i = R[\sin\theta_i \cos\varphi_i \hat{\mathbf{x}} + \sin\theta_i \sin\varphi_i \hat{\mathbf{y}} + \cos\theta_i \hat{\mathbf{z}}]. \tag{4}$$

The Euclidean distance between particles i and j is given by

$$r_{ij} = R\sqrt{2 - 2\hat{\mathbf{r}}_i \cdot \hat{\mathbf{r}}_j}, \tag{5}$$

where $\hat{\mathbf{r}}_i = \mathbf{r}_i/R$ is the versor that from the center of the sphere points towards the center of the ith particle.

The density of particles on the surface of the sphere is

$$\rho = \frac{N}{4\pi R^2}. \tag{6}$$

In the MC simulation [29] the RDF between two points on the sphere, $\mathbf{r}$ and $\mathbf{r}'$, is calculated through the following histogram estimator [see Eq. (A14)]

$$g(d) = \langle g^{\rm histogram}(d, \mathbf{R}) \rangle, \tag{7}$$

where $d = 2R\sin[\arccos(\hat{\mathbf{r}} \cdot \hat{\mathbf{r}}')/2]$ is the Euclidean distance between $\mathbf{r}$ and $\mathbf{r}'$, $\langle \ldots \rangle = \int_{S_R^N} \exp[-\beta U_N(\mathbf{R})] \ldots d\mathbf{R} / \int_{S_R^N} \exp[-\beta U_N(\mathbf{R})]\, d\mathbf{R}$ is the thermal average, here

$$U_N(\mathbf{R}) = \sum_{i<j} \phi(r_{ij}), \tag{8}$$

is the total potential energy of the fluid of particles, ϕ is the pair potential, and the integrals are taken in such way that $\mathbf{r}_i \in S_R$ for $i = 1, 2, \ldots, N$ with S_R the sphere of diameter $D = 2R$, so that $d\mathbf{R} = \prod_i d\mathbf{r}_i$ with $d\mathbf{r}_i = R^2 d\Omega_i = R^2 \sin\theta_i d\theta_i d\varphi_i$, and

$$g^{\rm histogram}(d, \mathbf{R}) = \sum_{i \neq j} \frac{1_{[d-\Delta/2, d+\Delta/2[}(r_{ij})}{N n_{id}(d)} \tag{9}$$

here $1_{[a,b[}(r) = 1$ if $r \in [a, b[$ and 0 otherwise, and

$$n_{id}(d) = N\left[\left(\frac{d + \Delta/2}{2R}\right)^2 - \left(\frac{d - \Delta/2}{2R}\right)^2\right], \tag{10}$$

is the average number of particles on the surface $[d-\Delta/2, d+\Delta/2[$ for the ideal gas of density ρ. $\rho^2 g(d)$ gives the probability that sitting on a particle at $\mathbf{r}$ one has to find another particle at $\mathbf{r}'$.

B. Experiment

The positional data of the particles in the colloidal cages is directly extracted from SEM images, which allowed the calculation of the particle separation for all visible particle pairs. Δ is set to an arbitrary value of $\sigma/20$. To exclude edge effects, a selection of particles located sufficiently at the center of the SEM image of the colloidal cage is taken into account. The RDF is determined from just one hemisphere. The particle positions from five SEM images of similar colloidal cages were used for the statistical average. The detailed procedure, the selection of particles, and validation of the procedure is described in our previous work [20]. In that work we calculated the radial distribution function from just one SEM image. Here we refined that analysis averaging the results from five SEM images, which is in spirit closer to the procedure used in the MC simulations. Although five images are still a rather small number our present procedure carries nevertheless more information than the one used in Ref. [20]. The absolute error on the experimental $g(r)$ is around 0.3. In the experiment unlike in the simulations each image measurement is uncorrelated from the other.

IV. MONTE CARLO RESULTS

We performed constant N, ρ, and T canonical MC simulations [29]. A typical run would consist of about $5\times10^5 N$ single-particle moves, keeping the acceptance ratios constant (≈ 0.3). In all the presented graphs of the simulated RDF the statistical error from the MC integration are not visible on the chosen scale.

We initially chose the PHS model pair potential to see how the RDF would change upon changing the temperature and the density. In order to find agreement with the experimental results it proved necessary to use the simpler HS model, as shown in Sec. V. We then compared the HS results with the soft-sphere model $\phi_{\rm SS}(r)=\epsilon_{\rm SS}(\frac{\sigma}{r})^6$ considered in Ref. [18]. For case "a" of Table I a reduced temperature of $k_BT/\epsilon_{\rm SS}=0.05$ is sufficient to have similar RDFs for the HS and the SS model on the half hemisphere, but when looking at the RDFs on the whole sphere, the SS RDF, unlike the HS one, shows relevant correlations between particles at opposite poles ($|g(2R)-1|\approx 0.3$).

TABLE I. Characteristics of the experimental colloidosomes analyzed. In all cases, the water droplet was of the same diameter $D=64.8\,\mu$m. Different colloidosomes differed by the diameter σ of the colloidal particles and by the number N of colloidal particles they carried. The same systems, "a", "b", "c", "d", have been studied through MC simulations.

case	σ (μm)	N	D/σ	$\rho\sigma^2$
a	4.80	561	13.5	0.98
b	3.32	1065	19.5	0.89
c	2.72	1498	23.8	0.84
d	2.56	1449	25.3	0.72

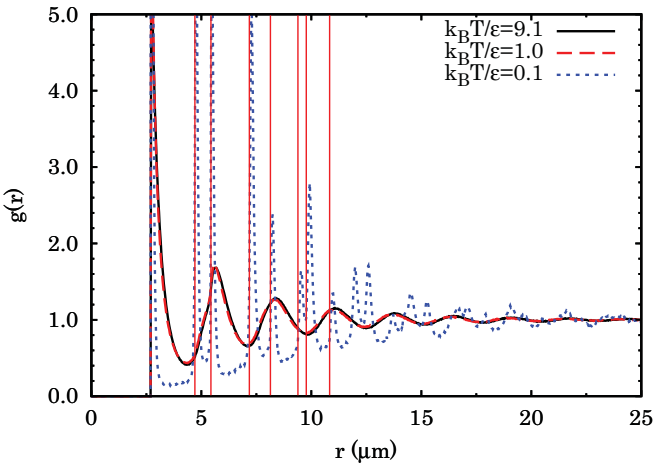

FIG. 2. (Color online) RDF for approximately one hemisphere of the colloidosome "c" of Table I with $N=1498$, $D/\sigma=23.8$, and various reduced temperatures, calculated with MC simulations of the PHS fluid. Also shown are the locations (vertical lines) of the first eight coordination shells of a regular planar hexagonal lattice of the hard-core particles (here $\sigma=2.72\,\mu$m). The mismatch between the peaks of the RDF and these shells is a manifestation of the curvature of the surface.

A. Dependence on temperature

The HS model is athermal so the structure is independent of temperature but only depends on the density. We thus simulated the colloidosome "c" in Table I with the PHS model. We chose different values of the reduced temperature, $k_BT/\epsilon_{\rm PHS}$ to see how the RDF would change.

As expected we found the occurrence of an ordered structure at small reduced temperatures (see Fig. 2). In particular we observe the formation of a regular hexagonal lattice distorted by the curvature of the spherical surface.

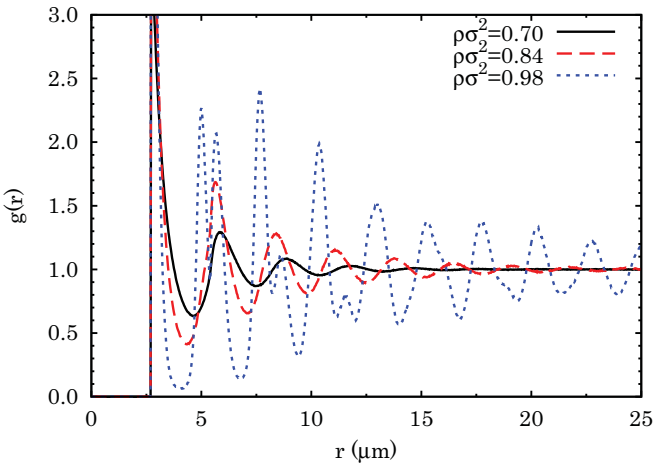

FIG. 3. (Color online) RDF for approximately one hemisphere of the colloidosome with $D/\sigma=23.8$ and $\sigma=2.72\,\mu$m at a reduced temperature $k_BT/\epsilon_{\rm PHS}=9.1$ and various densities, calculated with a MC simulation of the PHS fluid.

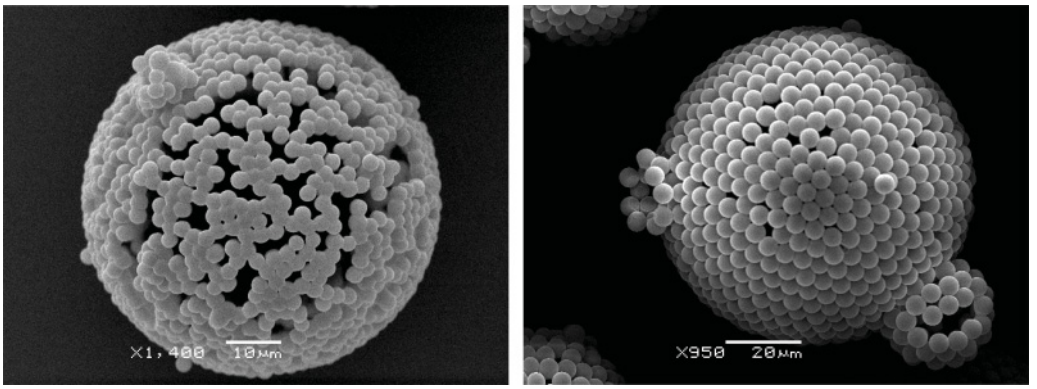

FIG. 4. SEM images of colloidal cages with a fluidlike particle configuration (left panel, $\rho\sigma^2 = 0.84$ and $D/\sigma = 23.8$) and a crystallinelike particle configuration (right panel, $\rho\sigma^2 = 0.98$ and $D/\sigma = 13.5$).

Recall that in a planar perfect hexagonal lattice arrangement of spheres of diameter σ the first coordination shells are as follows: $r/\sigma = 1, \sqrt{3}, 2, \sqrt{7}, 3, 2\sqrt{3}, \sqrt{13}, 4, \sqrt{19}, \sqrt{21}, 5, \ldots$.

From Fig. 2 we can clearly see how at this reduced density, 0.84, well below the maximum density, the PHS model reduces to the HS model for reduced temperatures $\gtrsim 1$. As we lower the temperature, the attractive tail in the pair potential starts to play a role resulting in a solidification of the fluid. As the fluid crystallizes, it may experience the cage effect going through glassy phases. The particles become confined in transient cages formed by their neighbors. This prevents them from diffusing freely on the surface of the sphere [30]. A related problem is the extremely long MC equilibration time necessary to draw the RDF of the figure at a temperature of 0.1, starting from a disordered initial configuration. In the limit of $T \to 0$, in our calculation, the equilibrium configuration of the (classical)

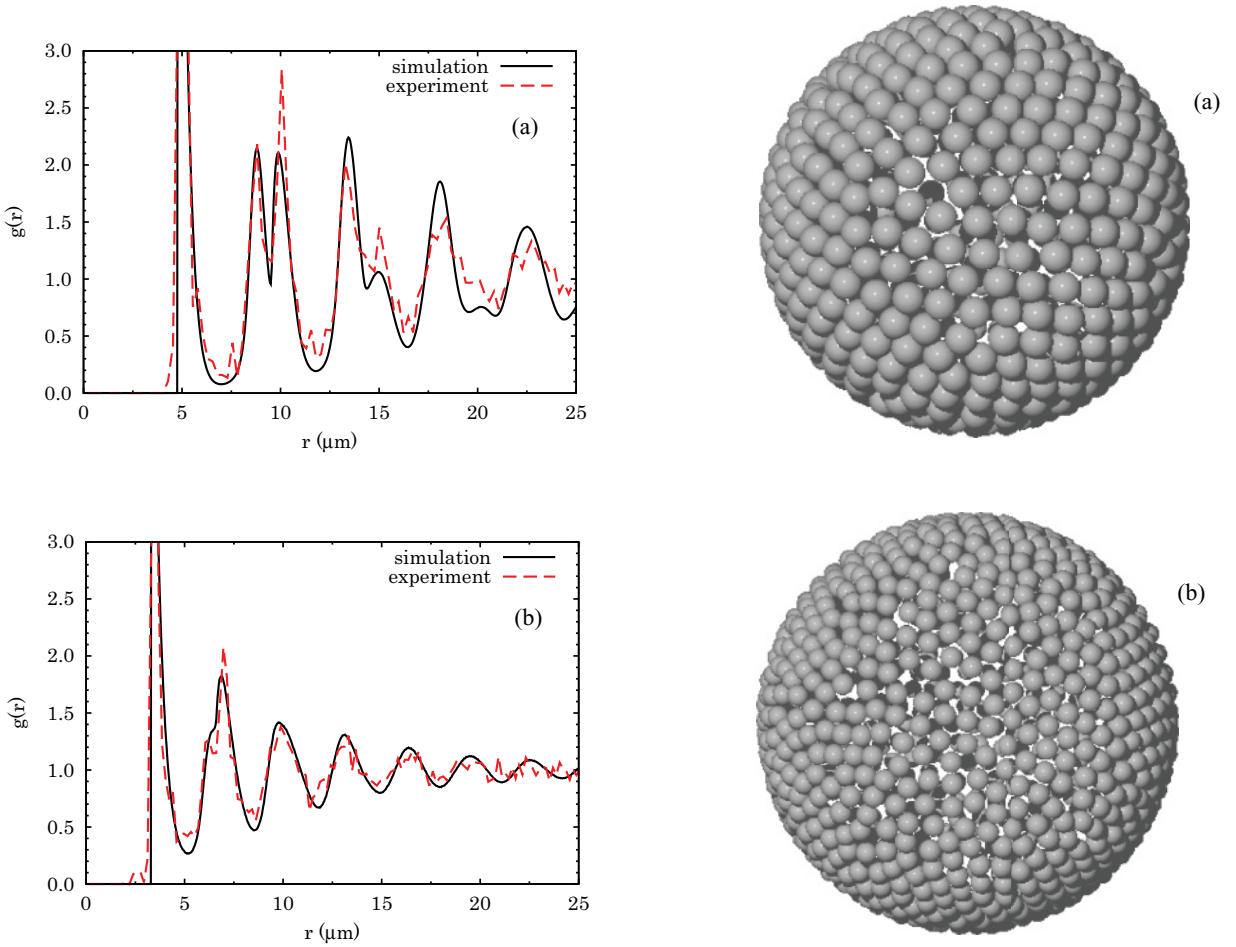

FIG. 5. (Color online) The experimental (dashed red line) and simulated (solid black line) RDF of colloidosomes "a" (top panel) and "b" (bottom panel) of Table I. The fluid model used in the MC simulations was the HS. The graphical representation of a snapshot of the particle positions when the MC has reached equilibrium, shows resemblance with the SEM images.

particles is the one $\mathbf{R}_0$ for which $U_N(\mathbf{R})$ has its minimum: the probability density is zero everywhere except on $\mathbf{R}_0$. We have a spontaneous breaking of the rotational symmetry (see Appendix A). The monotonously increasing tails in the PHS pair potential produce an equilibrium configuration with the particles forming one cluster of touching spheres. On the contrary, in the SS model the equilibrium configuration will be one where the interparticle spacing depends on the density.

B. Dependence on density

For case "c" in Table I ($D/\sigma = 23.8$ and $\sigma = 2.72\,\mu$m) we chose different values of the density to see how the RDF would change for the PHS model at a relatively high value of the reduced temperature $k_B T/\epsilon_{\text{PHS}} = 9.1$.

We succeeded in reaching high particle densities (without overlaps) by placing one particle at the north pole and then others centered at $\theta = 2n \arcsin(1/2R)$ and $\varphi = 2m \arcsin(1/2R \sin\theta)$ with $n,m = 1,2,3,\ldots$. This way we were, in particular, able to reach the 0.91 critical density observed by Prestipino Giarritta *et al.* [19] for HS. In doing so we observed the splitting of the second peak into a pair of adjacent peaks corresponding to the second and third coordination shells of a regular hexagonal lattice (see Fig. 3).

From Fig. 3 we can clearly see how the fluid tends to reach an ordered phase at high densities (even at high temperatures). The realization of these ordered phases will go through the formation of colloidal geometrical cages (due to geometrical frustration) on the surface of the water droplet, which is inevitable as the density slowly approaches the maximum density at any temperature.

V. COMPARISON BETWEEN EXPERIMENTAL AND MONTE CARLO SIMULATION RESULTS

The results of the experimental colloidosomes are now compared with the Monte Carlo (MC) simulations. Scanning Electron Microscopy (SEM) images of two different colloidal cages can be found in Fig. 4. The RDF of these colloidal cages and two others are shown in Figs. 5 and 6. The experimental colloidosomes studied differ from one another by particle size and particle density; the water droplets were of the same diameter and the temperature was room temperature, as summarized in Table I. The same values for number of particles, N, and sphere diameter, D/σ, are used in the MC simulations. Our first choice for the pair potential was the HS fluid model, as justified in Sec. II.

It is important to stress that in the experiment we measured the RDF from five images of different colloidal cages. Now,

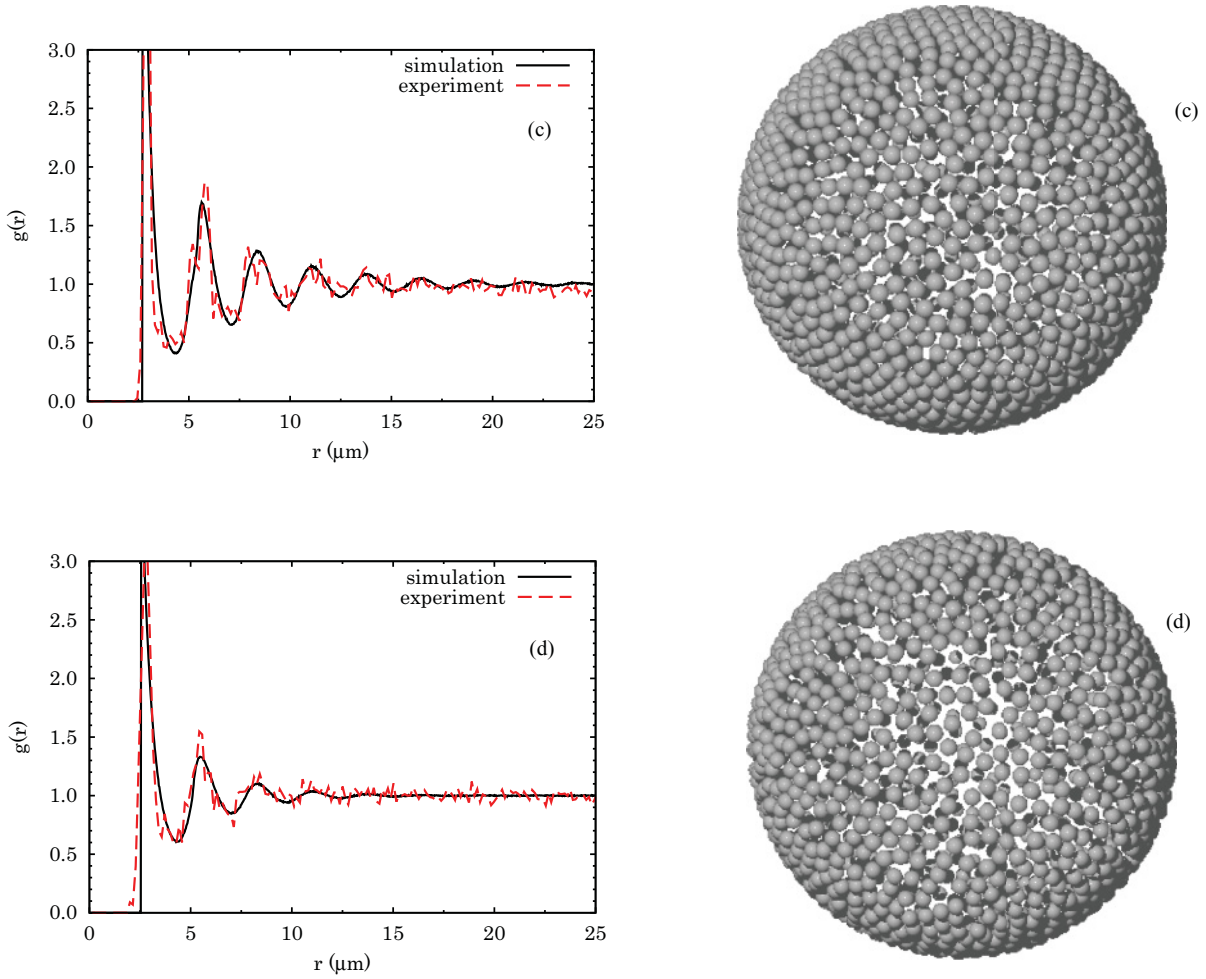

FIG. 6. (Color online) Same as Fig. 5 for the colloidosomes "c" (top panel) and "d" (bottom panel) of Table I.

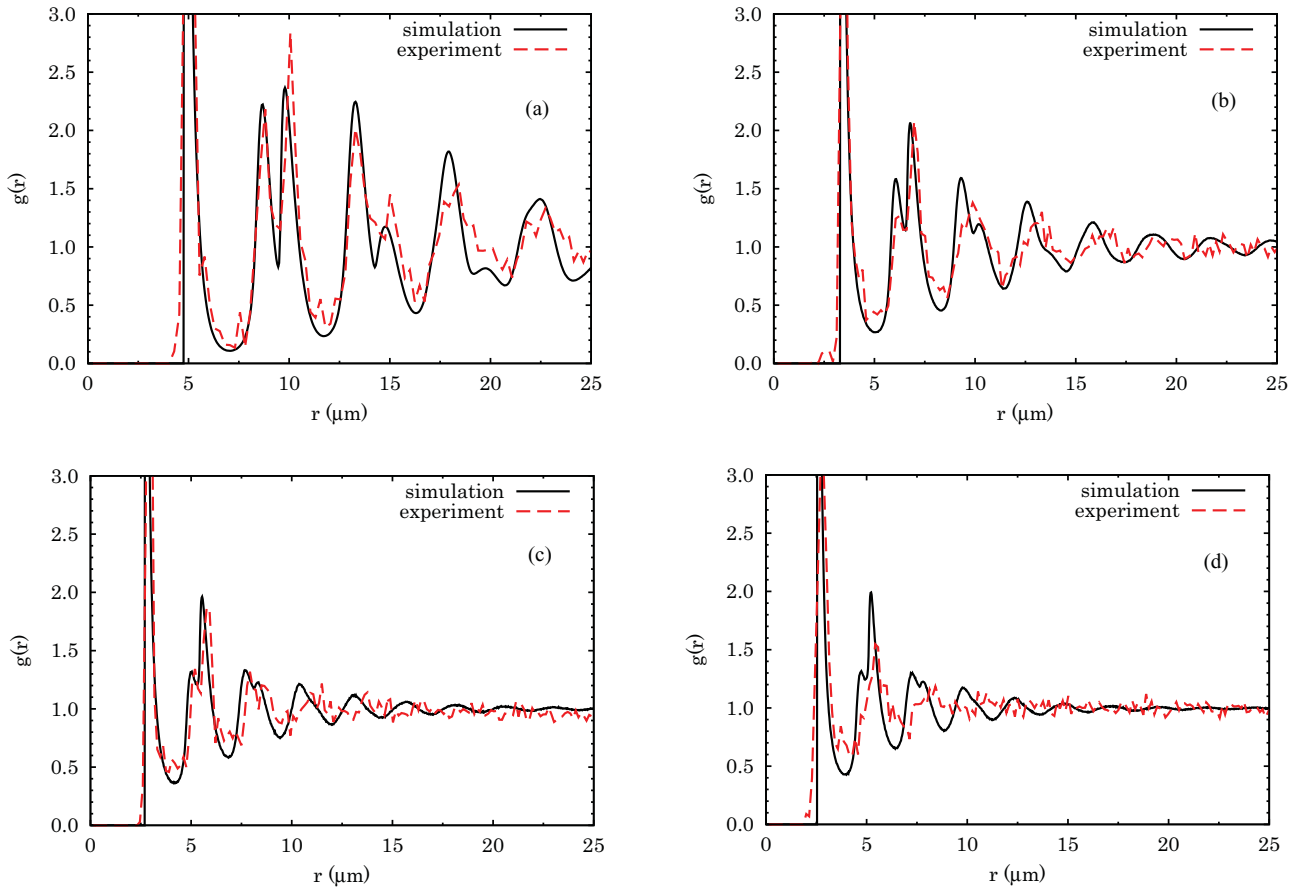

FIG. 7. (Color online) The experimental (dashed red line) and simulated (solid black line) RDF of colloidosomes "a", "b" (top panel) and "c", "d" (bottom panel) of Table I. The fluid model used in the MC simulations was the PHS with a reduced temperature of 0.3.

there are two processes responsible for the assembly of the particles on the colloidosome: (i) the adsorption of the particles on the interface at the moment of the formation of the Pickering emulsion and (ii) the motion of the particles on the interface. Our experimental measure is clearly not able to discriminate which one of the two processes is the more relevant, even if we expect that the structure of the colloidal cages obtained after the sintering procedure will carry no history of the former process. Moreover theoretical studies of process (i) are, to the best of our knowledge [31], much less developed than the ones of the latter. Our computer experiment only takes into account the second process assuming that the colloidosome is formed and the particles are in thermal equilibrium on the droplet.

From Figs. 5 and 6 we can see that there is a good agreement between the experimental and the theoretical RDF. This indicates that the HS fluid model gives a good description of the experimental system. The snapshots from the MC simulation of the colloidosome differ from the SEM images of the colloidal cages. The colloidal cages are formed by a network of touching particles. The structure of the experimental fluid points to a pretty strong short-range attraction between the particles mainly as a result of the sintering process. The measure of structure used, $g(r)$, is not sensitive to these structural differences.

We also simulated the experimental colloidosomes with the more realistic PHS model. Initially, the fluid with the highest particle density ("a") was used to adjust the reduced temperature. By trial and error we found that $k_BT/\epsilon_{\rm PHS} = 0.3$ gave a satisfying agreement with the experiment (see Fig. 7). However when we simulated the other colloidal cages with the same reduced temperature (the experimental temperature in all cases did not vary and the Hamaker constant did not change from one colloidosome to the other) we found disagreement between the MC simulation and the experiment as clearly shown by the last panel of Fig. 7. This is an indication that the particles used in the experiment do not interact as PHS. An explanation for this is the balance, in the oil phase, between the steric repulsion of the polymer chains and the Hamaker

TABLE II. Excess internal energy per particle $u^{\rm ex} = \langle U_N \rangle / N$ for the simulated PHS fluids on the sphere.

$k_BT/\epsilon_{\rm PHS}$	N	D/σ	$u^{\rm ex}/\epsilon_{\rm PHS}$
0.3	561	13.5	−2.1509(6)
0.3	1065	19.5	−1.862(3)
0.3	1498	23.8	−1.732(2)
0.3	1449	25.3	−1.586(3)
0.1	1498	23.8	−2.3484(8)
1.0	1498	23.8	−1.5450(4)
9.1	1498	23.8	−1.5136(3)
9.1	1747	23.8	−2.0932(2)
9.1	1248	23.8	−1.0741(2)

attraction. However, steric repulsion through the oil phase is unlikely, because pVP is insoluble in heptane. Another, possible explanation is that during emulsification the attractive interaction is balanced by the shear that is applied, and this could be reflected on the capsules structures sintered after the emulsification process.

In Table II we report the excess internal energy per particle measured in the MC simulations of the PHS model in the various systems studied. We can clearly see that as the fluid develops towards a solid phase there is a lowering of the energy.

VI. CONCLUSION

We have studied a colloidosome of polystyrene hairy particles of μm size moving on the surface of a water droplet in oil both experimentally and theoretically through canonical Monte Carlo simulations, which is the ensemble of choice for the description of the experimental system where the number of particles does not vary. In particular we studied the radial distribution function. Agreement was found between the experimental measure and the measure in the computer experiment of the theoretical model of the fluid of pure hard-sphere particles on the surface of a sphere. We did not find agreement between the experiment and the polarizable hard-sphere fluid model.

It would certainly be interesting to pursue a different determination of the radial distribution function through the imaging of the same colloidosome without going through the sintering procedure. This would allow an unbiased determination of the structure of the fluid of particles in their thermal equilibrium on the droplet surface.

Within the Monte Carlo simulation, a wide range of particle densities on the colloidosome was studied. At high density, the particles tend to arrange in a hexagonal lattice, distorted by the curvature of the droplet and the radial distribution function shows clear signatures of the first coordination shells. While at low densities a fluidlike behavior is manifested.

Our Monte Carlo simulation results further show that the addition of an attractive tail to the pure hard-sphere pair potential allows to reach solidification by lowering the temperature even at low densities. We discussed that for pair potentials with support on the whole $[0,2R]$, crystallization has to be expected at low temperatures at any density.

In our Monte Carlo study we have only considered direct interactions between the colloidal particles and not solvent-mediated indirect interactions, such as excluded volume depletion forces, the hairy hard-spheres interaction [32], or the Gourney solvation interaction, which depend on the thermodynamic state of the system [28]. We have simulated two fluid models on the spherical surface: the athermal HS one and the PHS one. By tuning the reduced temperature in the PHS model so as to get a structure similar to the one of the experimental case "a" of Table I, we were then unable to reproduce the experimental radial distribution function of the other cases "b", "c", and "d". Only the HS model agrees with all four experimental cases.

Our simulations show that the HS fluid model has small correlations between particles at opposite poles even at high densities [19], this is not any more so for particles with a soft core [18]. From the point of view of our work this remains just a theoretical prediction as our experimental measure of the radial distribution function is only able to probe half hemisphere. Moreover we expect the polystyrene particles used to be well described by the hard-core pair interaction. A further interesting comparison between the experiment and the simulation would be to compute the orientational correlation function Q_6 [33].

A possible further development of the work could be the realization of the binary mixture of small and large particles on the water droplet [34] to find experimental evidences for demixing predicted by the nonadditive hard-sphere model with negative nonadditivity [35]. Or as a possible way to push the fluidlike behavior at larger densities, diminishing the glass gap, as predicted by the additive hard-sphere model [36]. A natural extension would then be the multicomponent mixture, which in its polydisperse limit may leave no space to the glass. It would also be possible to simulate the particles as penetrable-square-well ones [37].

Colloidosomes may be used to isolate viruses when at the moment of the formation of the Pickering emulsion only one is captured inside each droplet. This may be a way to overcome the usual staining procedure. Of course the opposite situation may also be possible when many living cells, for example eukaryotic flagella [38], coordinate themselves in the confined geometry of the drop.

ACKNOWLEDGMENTS

The MC simulations were carried out at the Center for High Performance Computing (CHPC), Council of Scientific and Industrial Research (CSIR) Campus, South Africa. B.K. acknowledges support by the South African Research Chairs Initiative of the Department of Science and Technology and National Research Foundation.

APPENDIX A: PAIR CORRELATION FUNCTION

Given a classical system of N particles of mass m moving in a region $\mathcal{R}$ of a Riemannian manifold of dimension d and metric tensor $g_{\mu\nu}(\mathbf{q})$ with Hamiltonian,

$$\mathcal{H}_N = \mathcal{T}_N + \mathcal{U}_N, \tag{A1}$$

$$\mathcal{T}_N = \frac{1}{2m}\sum_{i=1}^{N} g^{\mu\nu}(\mathbf{q}_i)p_{i\mu}p_{i\nu}, \tag{A2}$$

$$\mathcal{U}_N = U_N(\mathbf{q}_1,\ldots,\mathbf{q}_N), \tag{A3}$$

where we denote with $\mathbf{q} = (q^1,\ldots,q^d)$ a point of the manifold, with $\mathbf{q}_i = (q_i^1,\ldots,q_i^d)$ the coordinates of particle i and with $\mathbf{p}_i = (p_{i1},\ldots,p_{id})$ its canonically conjugate momenta, and we use the Einstein summation convention to omit the sum over the repeated Greek indices. The canonical ensemble probability density to find the statistical system of distinguishable particles, the fluid, in thermal equilibrium at an inverse temperature $\beta = 1/k_BT$ (with k_B Boltzmann constant) with coordinates $\mathbf{Q} = (\mathbf{q}_1,\ldots,\mathbf{q}_N)$ and momenta $\mathbf{P} = (\mathbf{p}_1,\ldots,\mathbf{p}_N)$ is

$$\mathcal{F}(\mathbf{Q},\mathbf{P},N) = \frac{1}{\Theta}\frac{1}{h^{dN}N!}e^{-\beta(\mathcal{T}_N+\mathcal{U}_N)}, \tag{A4}$$

where h is Planck constant and the normalization factor Θ is the partition function of the canonical ensemble of the

identical particles

$$\Theta = \frac{1}{h^{dN}N!}\int_{\mathcal{R}^N} d\mathbf{Q}\int d\mathbf{P} e^{-\beta(\mathcal{T}_N+\mathcal{U}_N)} = \frac{1}{\Lambda^{dN}N!}\int_{\mathcal{R}^N} d\mathbf{V} e^{-\beta\mathcal{U}_N} = e^{-\beta F}, \tag{A5}$$

where in the second equality we performed the Gaussian integral over the conjugated momenta so that $d\mathbf{V} = d\mathbf{v}_1\cdots d\mathbf{v}_N$ with $d\mathbf{v}_i = \sqrt{g}\prod_{\mu=1}^{d} dq_i^\mu$ (here $g = \det||g_{\mu\nu}(\mathbf{q}_i)|| = [\det||g^{\mu\nu}(\mathbf{q}_i)||]^{-1}$) the infinitesimal volume element of the manifold and $\Lambda = \sqrt{2\pi\beta\hbar^2/m}$ is the de Broglie thermal wavelength. To justify a classical treatment of the statistical properties it is necessary that Λ be much less than the mean nearest neighbor distance between the particles. In the last equality we used the definition of entropy and F is the Helmholtz free energy.

If the particles move on a sphere of radius one, $\mathcal{R} = S_1$, then the coordinates are the polar coordinates on the sphere $\mathbf{q}_i = (\theta_i,\varphi_i)$ with $\theta_i \in [0,\pi]$ the polar angle and $\varphi_i \in [0,2\pi)$ the azimuthal angle, and the metric tensor is

$$||g_{\mu\nu}(\mathbf{q})|| = \begin{pmatrix} 1 & 0 \\ 0 & \sin^2\theta \end{pmatrix}, \tag{A6}$$

so that $\det||g_{\mu\nu}(\mathbf{q}_i)|| = \sin^2\theta_i$ and $d\mathbf{v}_i = \sin\theta_i d\theta_i d\varphi_i \equiv d\Omega_i$ the solid angle spanned by the three-dimensional vector $\mathbf{r}_i$ of the position of particle i in the Euclidean space with origin on the sphere center. Given a physical observable only function of the coordinates $\mathcal{O}_N = O_N(\mathbf{Q})$, we can then measure its average value as

$$\langle\mathcal{O}_N\rangle = \frac{\int_{\mathcal{R}^N} O_N(\mathbf{Q}) e^{-\beta U_N(\mathbf{Q})}\prod_{i=1}^{N} d\mathbf{v}_i}{\int_{\mathcal{R}^N} e^{-\beta U_N(\mathbf{Q})}\prod_{i=1}^{N} d\mathbf{v}_i}. \tag{A7}$$

For example the one-body correlation function [39] for the particles on a sphere of radius R is measured as

$$\rho(\mathbf{q}) = \left\langle \sum_{i=1}^{N} \frac{\delta^{(2)}(\mathbf{q},\mathbf{q}_i)}{R^2}\right\rangle, \tag{A8}$$

where $\delta^{(2)}(\mathbf{q},\mathbf{q}') = \delta(\theta-\theta')\delta(\varphi-\varphi')/\sqrt{g}$ is the Dirac δ function on the manifold. We now use the fact that our potential energy (8) is invariant under any rotation of the reference frame to say that $\rho(\mathbf{q})$ has to be independent of $\mathbf{q}$ and [by integrating (A8) over $d\mathbf{v}$] we must have $\rho(\mathbf{q}) = \rho = N/(4\pi R^2)$.

The two-body correlation function [39] is measured as

$$g(\mathbf{q},\mathbf{q}') = \left\langle \sum_{i\neq j} \frac{\delta^{(2)}(\mathbf{q},\mathbf{q}_i)}{R^2}\frac{\delta^{(2)}(\mathbf{q}',\mathbf{q}_j)}{R^2}\right\rangle \Bigg/ [\rho(\mathbf{q})\rho(\mathbf{q}')]\,. \tag{A9}$$

Because of rotational invariance g can only depend on the geodesic distance d between $\mathbf{q}$ and $\mathbf{q}'$. We can then calculate it on a reference frame where $\varphi = \varphi'$ so that $d = R(\theta-\theta')$ and

$$g(d) = \left\langle \sum_{i\neq j} \frac{\delta(\theta-\theta_i)}{R^2\sin\theta_i}\frac{\delta(\theta'-\theta_j)}{\sin\theta'}\delta(\varphi'-\varphi_i)\delta(\varphi'-\varphi_j)\right\rangle \Bigg/ \times(R^2\rho^2). \tag{A10}$$

If we now choose $\theta = \bar\theta + \theta'$ and integrate over $d\mathbf{v}'$ we get

$$g(d) = \left\langle \sum_{i\neq j} \frac{\delta(\bar\theta-\theta_{ij})}{R^2\sin\theta_i}\delta(\varphi_{ij})\right\rangle \Bigg/ (N\rho), \tag{A11}$$

where $\theta_{ij} = \theta_i - \theta_j$ and $\varphi_{ij} = \varphi_i - \varphi_j$. We can use rotational invariance to choose the sphere north pole sitting on particle j to get further

$$g(d) = \left\langle \sum_{i\neq j} \delta(\bar\theta-\theta_{ij})\delta(\varphi_{ij})\right\rangle \Bigg/ (N\rho R^2\sin\bar\theta). \tag{A12}$$

In place of the geodesic distance $R\bar\theta$ we can use the Euclidean distance $d = 2R\sin(\bar\theta/2)$. We can then use the equality $\delta(\bar\theta-\theta_{ij}) = \delta(d-d_{ij})R\cos(\bar\theta/2)$, here $d_{ij} = 2R\sin(\theta_{ij}/2)$, to write

$$g(d) = \left\langle \sum_{i\neq j} \delta(d-d_{ij})\delta(\varphi_{ij})\right\rangle \Bigg/ (N\rho d) = \left\langle \sum_{i\neq j} \delta(d-r_{ij})\delta(\varphi_{ij})\right\rangle \Bigg/ (N\rho d), \tag{A13}$$

where r_{ij} is defined in Eq. (5) of the main text. Now we use rotational invariance noticing again that given any two point $\mathbf{q}_i$ and $\mathbf{q}_j$ on the sphere one can always find a reference frame in which $\varphi_i = \varphi_j$ to get

$$g(d) = \left\langle \sum_{i\neq j} \delta(d-r_{ij})\right\rangle \Bigg/ (N\rho 2\pi d). \tag{A14}$$

APPENDIX B: MONTE CARLO SIMULATION

In the Monte Carlo integration one does a random walk [40] in $\mathbf{Q}$ with $\theta_i \in [0,\pi], \varphi_i \in [-\pi/2,\pi/2)$ for all $i = 1,\ldots,N$ with periodic boundary conditions: $\varphi = \varphi + 2\pi$ and $\theta = \theta + \pi$. In the Metropolis algorithm [40] one takes as the acceptance probability

$$A[\mathbf{Q}\to\mathbf{Q}'] = \min\left\{1, e^{-\beta[U_N(\mathbf{Q}')-U_N(\mathbf{Q})]}\frac{\prod_{i=1}^{N}\sin\theta_i'}{\prod_{i=1}^{N}\sin\theta_i}\right\}. \tag{B1}$$

[1] A. D. Dinsmore *et al.*, Science **298**, 1006 (2002); C. Zeng, H. Bissig, and A. D. Dinsmore, Solid State Comm. **139**, 547 (2006); A. B. Subramanian, M. Abkarian, and H. A. Stone, Nature Mat. Lett. **4**, 553 (2005).

[2] R. F. Lee, Spill Science and Technology Bulletin **5**, 117 (1999); E. Dickinson, Curr. Opin. Colloid Interface Sci. **15**, 40 (2010); D. Rousseau, S. Ghosh, and H. Park, J. Food. Sci. **74**, E1 (2009); S. Lu, R. J. Pugh, and E. Forssberg, in *Interfacial Separation of Particles*, Vol. 20 (Elsevier, Amsterdam, 2005); J. Frelichowska, M. A. Bolzinger, J. Pelletier, J. P. Valour, and Y. Chevalier, International Journal of Pharmaceutics **371**, 56 (2009); P. H. F. Hansen, S. Rödner, and L. Bergström, Langmuir **17**, 4867 (2001).

[3] P. Binks and T. S. Horozov, *Colloidal Particles at Liquid Interfaces* (Cambridge University Press, Cambridge, 2006); L. Hong, S. Jiang, and S. Granick, Langmuir **22**, 9495 (2006).

[4] S. A. F. Bon and T. Chen, Langmuir **23**, 9527 (2007).

[5] E. Pitard, M. L. Rosinberg, G. Stell, and G. Tarjus, Phys. Rev. Lett. **74**, 4361 (1995).

[6] Isabelle Cantat, Sylvie Cohen-Addad, Florence Elias, François Graner, Renihard Höhler, Olivier Pitois, Florence Rouyer, and Arnaud Saint-Jalmes, *Les mousses: structure et dynamique* (Belin, Paris, 2010).

[7] P. Pieranski, Phys. Rev. Lett. **45**, 569 (1980); R. Aveyard *et al*., *ibid*. **88**, 246102 (2002); M. E. Leunissen *et al*., Proc. Nat. Acad. Sci. USA **104**, 2585 (2007); K. Masschaele, B. J. Park, E. M. Furst, J. Fransaer, and J. Vermant, Phys. Rev. Lett. **105**, 048303 (2010); J. Guzowski, M. Tasinkevych, and S. Dietrich, Phys. Rev. E **84**, 031401 (2011).

[8] M. Bowick, A. Cacciuto, D. R. Nelson, and A. Travesset, Phys. Rev. Lett. **89**, 185502 (2002); M. K.-H. Kiessling, J. Stat. Phys. **136**, 275 (2009).

[9] J. M. Caillol, J. Phys. Lett. **42**, L245 (1981).

[10] A. R. Bausch *et al*., Science **299**, 1716 (2003).

[11] P. Lipowsky, M. J. Bowick, J. H. Meinke, D. R. Nelson, and A. R. Bausch, Nature Mat. **4**, 407 (2005).

[12] M. J. Bowick, D. R. Nelson, and A. Travesset, Phys. Rev. B **62**, 8738 (2000).

[13] S. Sastry, D. S. Corti, P. G. Debenedetti, and F. H. Stillinger, Phys. Rev. E **56**, 5524 (1997).

[14] M. J. Bowick and L. Giomi, Adv. Phys. **58**, 449 (2009).

[15] C. N. Likos, Phys. Rep. **348**, 267 (2001); E. Zaccarelli, J. Phys.: Condens. Matter **19**, 323101 (2007).

[16] R. Fantoni, B. Jancovici, and G. Téllez, J. Stat. Phys. **112**, 27 (2003).

[17] R. Fantoni and G. Téllez, J. Stat. Phys. **133**, 449 (2008).

[18] F. Sausset, G. Tarjus, and D. R. Nelson, Phys. Rev. E **81**, 031504 (2010); M. Chávez-Páez *et al*., J. Chem. Phys. **119**, 7461 (2003); P. X. Viveros-Méndez, J. M. Méndez-Alcaraz, and P. González-Mozuelos, *ibid*. **128**, 014701 (2008).

[19] S. Prestipino Giarritta, M. Ferrario, and P. V. Giaquinta, Physica A **187**, 456 (1992); **201**, 649 (1993).

[20] J. W. O. Salari, G. T. Jemwa, H. M. Wyss, and B. Klumperman, Soft Matter **7**, 2033 (2011); J. W. O. Salari, Ph.D. thesis, Eindhoven University of Technology, 2011 (unpublished).

[21] C. E. Smith, J. Phys.: Conf. Ser. **237**, 012021 (2010); L. Bruneau and S. De Bièvre, Comm. Math. Phys. **229**, 511 (2002).

[22] S. U. Pickering, J. Chem. Soc. **91**, 2001 (1907).

[23] J. W. O. Salari, F. A. M. Leermakers, and B. Klumperman, Langmuir **27**, 6574 (2011), and references therein.

[24] L. D. Landau and E. M. Lifshitz, *Quantum Mechanics. Non-relativistic Theory*, 3rd ed., Vol. 3 (Pergamon Press, Oxford, 1977), course of Theoretical Physics. Sec. 89.

[25] H. C. Hamaker, Physica **4**, 1058 (1937).

[26] Suppose that the particles had a sticky-hard-sphere interaction [41] the surface adhesion would still be canceled by the presence of the hairs.

[27] S. Jiang and S. Granick, Langmuir **24**, 2438 (2008).

[28] D. Gazzillo, A. Giacometti, R. Fantoni, and P. Sollich, Phys. Rev. E **74**, 051407 (2006).

[29] M. P. Allen and D. J. Tildesley, *Computer Simulation of Liquids* (Clarendon Press, Oxford, 1987); D. Frenkel and B. Smit, *Understanding Molecular Simulation* (Academic Press, San Diego, 1996).

[30] E. R. Weeks and D. A. Weitz, Chem. Phys. **284**, 361 (2002).

[31] Grazyna Antczak and Gert Ehrlich, *Surface Diffusion: Metals, Metal Atoms, and Clusters* (Cambridge University Press, Cambridge, 2010).

[32] E. W. Fischer, Kolloid Z. **160**, 120 (1958).

[33] P. R. ten Wolde, M. J. Ruiz-Montero, and D. Frenkel, J. Chem. Phys. **104**, 9932 (1996).

[34] A. D. Law, D. M. A. Buzza, and T. S. Horozov, Phys. Rev. Lett. **106**, 128302 (2011).

[35] A. Santos, M. L. de Haro, and S. B. Yuste, J. Chem. Phys. **132**, 204506 (2010); R. Fantoni and A. Santos, Phys. Rev. E **84**, 041201 (2011).

[36] A. Santos, S. B. Yuste, M. L. de Haro, J. Chem. Phys. **135**, 181102 (2011).

[37] R. Fantoni, A. Giacometti, A. Malijevský, and A. Santos, J. Chem. Phys. **131**, 124106 (2009).

[38] R. E. Goldstein, M. Polin, and I. Tuval, Phys. Rev. Lett. **107**, 148103 (2011).

[39] T. L. Hill, *Statistical Mechanics* (McGraw-Hill, New York, 1956).

[40] M. H. Kalos and P. A. Whitlock, *Monte Carlo Methods* (Wiley, Weinheim, 2008).

[41] R. Fantoni, D. Gazzillo, and A. Giacometti, J. Chem. Phys. **122**, 034901 (2005); Phys. Rev. E **72**, 011503 (2005).